nature neuroscience

Scaling down of balanced excitation and inhibition by active behavioral states in auditory cortex

Mu Zhou[1–3,6], Feixue Liang[1,4,6], Xiaorui R Xiong[1,3], Lu Li[4], Haifu Li[4], Zhongju Xiao[4], Huizhong W Tao[1,5] & Li I Zhang[1,2]

Cortical sensory processing is modulated by behavioral and cognitive states. How this modulation is achieved by changing synaptic circuits remains largely unknown. In awake mouse auditory cortex, we found that sensory-evoked spike responses of layer 2/3 (L2/3) excitatory cells were scaled down with preserved sensory tuning when mice transitioned from quiescence to active behaviors, including locomotion, whereas L4 and thalamic responses were unchanged. Whole-cell voltage-clamp recordings revealed that tone-evoked synaptic excitation and inhibition exhibited a robust functional balance. The change to active states caused scaling down of excitation and inhibition at approximately equal levels in L2/3 cells, but resulted in no synaptic changes in L4 cells. This lamina-specific gain control could be attributed to an enhancement of L1-mediated inhibitory tone, with L2/3 parvalbumin inhibitory neurons also being suppressed. Thus, L2/3 circuits can adjust the salience of output in accordance with momentary behavioral demands while maintaining the sensitivity and quality of sensory processing.

The processing of sensory information in cortical neurons is achieved through the spatiotemporal integration of converging synaptic inputs evoked by sensory stimuli[1–3]. Such synaptic integration is largely determined by the structure of the underlying functional cortical synaptic circuits[2,4,5], but can also be influenced by the behavioral and cognitive states of the animal[6–11], which modulate the internally generated brain activities[12–15]. In visual and somatosensory cortices, it has been shown that behaviorally active states, such as locomotion and whisking, result in a depolarization of the membrane potential and a more desynchronized state of cortical neurons[16–18], which alters the level or reliability of their spike responses to sensory stimulation[8,11,17–19]. Despite the observed changes in membrane potential dynamics, the manner in which behavioral states directly modulate cortical synaptic circuits, as reflected by potential changes of excitatory and inhibitory synaptic inputs to a cortical neuron, remains largely unknown.

Using high-quality *in vivo* whole-cell voltage-clamp recordings in awake head-fixed mice, we recorded excitatory and inhibitory synaptic inputs to the same cortical neurons under different behavioral states of the animal. In middle layers of the primary auditory cortex (A1), we found a robust functional balance between sound-evoked excitatory and inhibitory inputs to a cortical neuron under various behavioral states, which is a salient synaptic circuit property that has been demonstrated in anesthetized animal models[2,20–23]. The balanced synaptic excitation and inhibition were found to be scaled down at a similar level during active states as compared with the quiet resting state in L2/3, but not L4, excitatory cells, resulting in well-preserved sensory tuning of the former cells. We also found that layer 1 (L1) interneurons were activated in active states, which contributed to the reduced response gain of L2/3 excitatory cells. Together, our results suggest that balanced excitation and inhibition is a fundamental synaptic circuit basis for auditory cortical processing in the awake A1, and that behavioral state–dependent scaling of excitatory and inhibitory inputs may be a general strategy for cortical circuits to adjust the representation of sensory information according to momentary behavioral and task demands.

RESULTS

Lamina-specific downregulation of auditory responses

We first examined whether and how auditory cortical responses are modulated by changes of behavioral state in awake head-fixed mice habituated to rest or run on a flat rotatable plate (Online Methods). The behavior of the animal was monitored with a video camera and the speed of the rotation of the plate was recorded in real time (**Fig. 1a**). The mice displayed three identifiable behavioral states (**Fig. 1b**): quiescence (Q, quiet resting), active without locomotion (A – L, whisking and/or facial, jaw or paw movements) and locomotion (L, running). During locomotion, the mouse also whisked. These behavioral states correlated well with different speeds of plate rotation (**Fig. 1b**,**c**). The A – L state caused small back and forth movements of the plate, the speed of which was clearly distinguished from that caused by locomotion (**Fig. 1c**). The power spectrum of the local field potential (LFP) recorded in the A1 (**Fig. 1d**) showed an increase in the power of high-frequency oscillations (20–80 Hz) and a decrease in the power of low-frequency oscillations (1–10 Hz) during both the A – L and L states as compared with the Q state (**Fig. 1e**,**f**, and **Supplementary Fig. 1**),

[1]Zilkha Neurogenetic Institute, University of Southern California, Los Angeles, California, USA. [2]Department of Physiology and Biophysics, University of Southern California, Los Angeles, California, USA. [3]Graduate Programs, Keck School of Medicine, University of Southern California, Los Angeles, California, USA. [4]Department of Physiology, School of Basic Medical Sciences, Southern Medical University, Guangzhou, China. [5]Department of Cell and Neurobiology, University of Southern California, Los Angeles, California, USA. [6]These authors contributed equally to this work. Correspondence should be addressed to L.I.Z. (liizhang@usc.edu), Z.X. (xiaozj@fimmu.com) or H.W.T. (htao@usc.edu).

Received 26 January; accepted 24 March; published online 20 April 2014; doi:10.1038/nn.3701

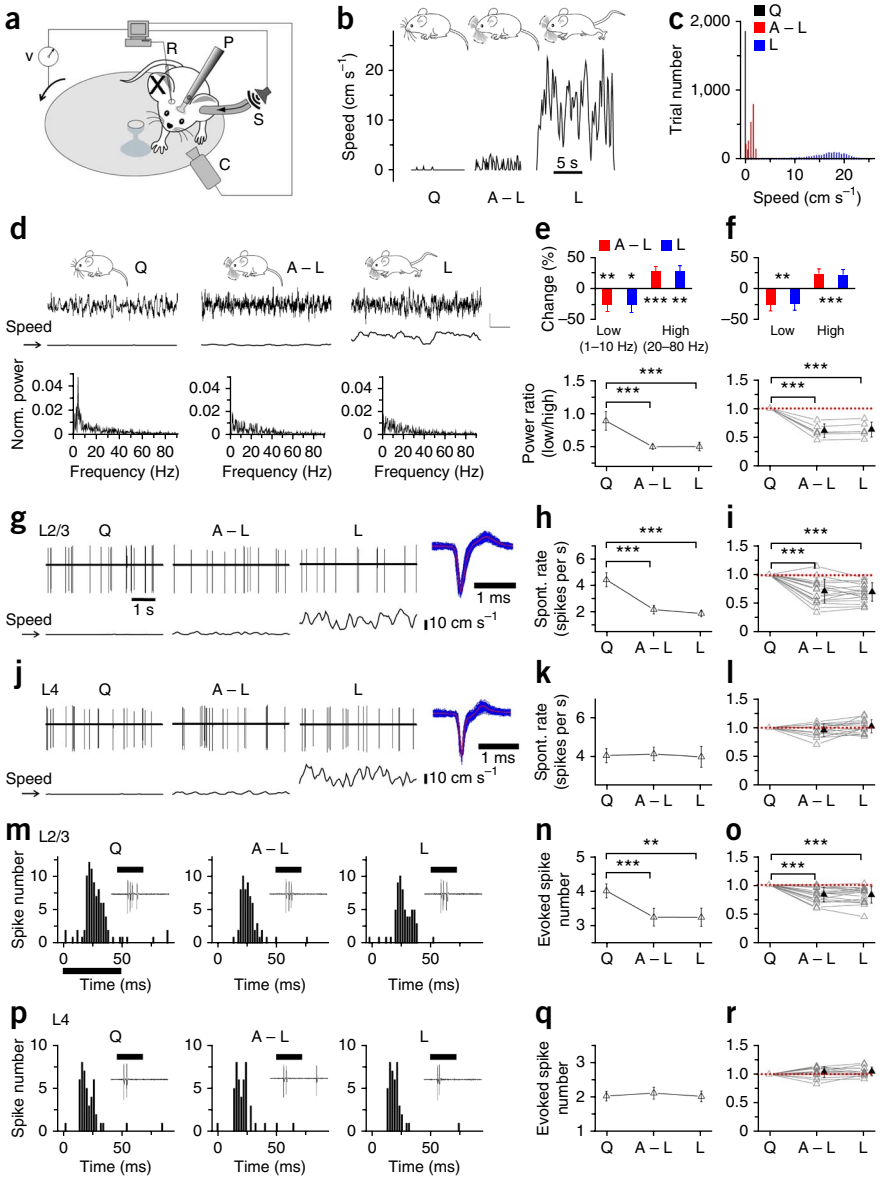

Figure 1 Behavioral state–dependent modulation of spike responses in the mouse A1. (**a**) Experimental setup. R, recording electrode; P, head-fixation post; S, sound stimulation; C, camera; v, velocity meter. (**b**) Sample records of plate rotation speed in different behavioral states. (**c**) Distribution of average speeds (in a 1-s epoch) in randomly sampled 2,000 epochs ($n = 3$ mice). (**d**) Top, sample records of LFP in the A1. Middle, simultaneously recorded plate rotating speed. Arrow indicates speed at 0. Scale bars represent 250 μV and 0.5 s (top) and 20 cm s^{-1} and 0.5 s (bottom). Bottom, power spectrum of LFP. (**e**) Top, percentage change in power of low-frequency (1–10 Hz) and high-frequency (20–80 Hz) components of LFP relative to quiescence, for the recording shown in **d**. Power spectrums were generated for each 3.3-s segment of LFP records. $N = 5$ segments. From left to right, t test ($P = 0.0035$, $t = -5.118$), Wilcoxon signed-rank test ($P = 0.0313$, $Z = -1.888$), t test ($P = 0.0006$, $t = 8.268$), t test ($P = 0.0012$, $t = 6.865$). Bottom, the ratio of power of the low versus high-frequency component. One-way ANOVA ($P = 6.68 \times 10^{-6}$, $F = 37.73$) and *post hoc* test. (**f**) Summary of recordings in six mice. Power ratio was normalized by the average value in the Q state. Top, t test ($P = 0.0011$, 0.0016, 0.0003 and 0.0006; $t = -5.802$, -5.302, 7.453 and 6.637, respectively). Bottom, one-way ANOVA ($P = 1.75 \times 10^{-5}$, $F = 24.80$) and *post hoc* test. (**g**–**i**) Spontaneous firing in L2/3 neurons in different states. (**g**) Top, records of spontaneous spikes of a L2/3 excitatory cell. Bottom, simultaneously recorded plate rotation speed. Arrow indicates speed at 0. Right inset, superimposed 500 individual spikes (blue) and the average spike shape (red). (**h**) Average spontaneous spike rates in the same cell. One-way ANOVA ($P = 1.26 \times 10^{-5}$, $F = 12.88$, $n = 30$ 5-s segments.) and *post hoc* test. (**i**) Summary of 17 recorded L2/3 excitatory cells. Spike rate was normalized by the average value in the Q state. One-way ANOVA ($P = 2.66 \times 10^{-7}$, $F = 21.10$) and *post hoc* test. (**j**–**l**) Spontaneous spikes recorded in L4 excitatory cells. Data are presented as in **g**–**i**. (**k**) One-way ANOVA ($P = 0.9841$, $F = 0.0160$, $n = 28$ segments) and *post hoc* test. (**l**) One-way ANOVA ($P = 0.1542$, $F = 1.955$, $n = 15$) and *post hoc* test. (**m**) Peri-stimulus spike time histogram (PSTH, bin size = 1 ms) for the responses of a L2/3 excitatory cell to CF tones (black lines) in different states. Inset, sample record of evoked spikes by the tone. (**n**) Average evoked spike number per stimulus trial plotted for the same cell. Error bars represent s.d. One-way ANOVA ($P = 1.21 \times 10^{-5}$, $F = 12.93$, $n = 25$ trials) and *post hoc* test. (**o**) Summary of average evoked spike numbers for 17 similarly recorded L2/3 excitatory cells. One-way ANOVA ($P = 1.89 \times 10^{-5}$, $F = 13.76$) and *post hoc* test. (**p**,**q**) Evoked spike responses of a L4 excitatory cell. $N = 25$ trials. One-way ANOVA ($P = 0.7415$, $F = 0.3004$) and *post hoc* test. (**r**) Summary of average evoked spike numbers for 15 recorded L4 cells. One-way ANOVA ($P = 0.1708$, $F = 1.844$) and *post hoc* test. $^*P < 0.05$, $^{**}P < 0.01$, $^{***}P < 0.001$. Error bars represent s.d. in all panels.

consistent with previous reports that locomotion or whisking can result in a desynchronized brain state[11–13]. After determining the location of the A1 with extracellular recordings, we performed *in vivo* cell-attached loose-patch recordings from individual A1 neurons (Online Methods). We recorded both the spontaneous and sound-evoked spikes of the cells. Cells in this recorded population were presumed excitatory cells, as they all exhibited broad spike shapes[24] (**Fig. 1g**). Compared with the Q state, the A – L and L states similarly reduced the spontaneous firing rate in L2/3 neurons (**Fig. 1g–i**), but did not affect it in L4 neurons (**Fig. 1j–l**, see **Supplementary Fig. 2** for layer assignment). This L2/3-specific decrease in spontaneous activity is reminiscent of a previous report in rat auditory cortex that spontaneous activity of superficial neurons is suppressed during cortical desynchronization[25]. Furthermore, the A – L and L states similarly reduced the spiking response to the characteristic frequency (CF) tone in L2/3 neurons as compared with the Q state (**Fig. 1m–o**), whereas, in L4 neurons, the CF tone–evoked spiking activity was not affected by the changes of behavioral state (**Fig. 1p–r**). Thus, different from the observations in the visual cortex[11,18,19], where locomotion results in enhanced sensory-evoked activity in both L2/3 and L4, the auditory cortex exhibited a lamina-specific downregulation of sensory-evoked responses. In addition, it is worth mentioning that both the spontaneous and evoked firing rates were higher during the awake quiescence state than during the urethane-anesthetized state

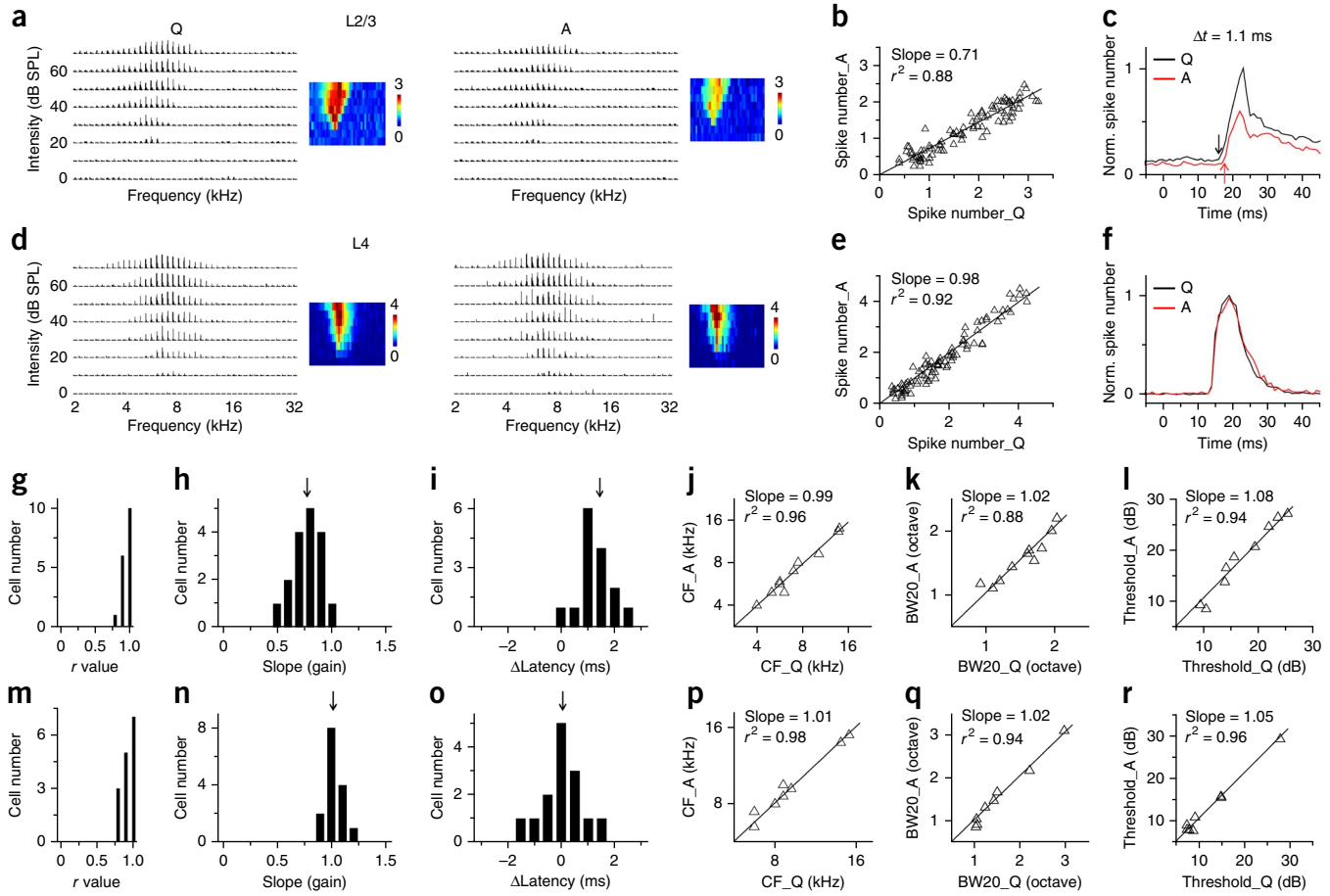

Figure 2 Gain modulation of auditory responses by behavioral state. (**a**) TRFs of spike responses of a L2/3 cell in quiescence (Q) and active (A) states. Each element in the array represents the PSTH of evoked spikes (60-ms time window, bin size = 2 ms, ten repeats) to the corresponding tone stimulus. Color map depicts the average spike number evoked by tones. (**b**) Evoked spike number by a tone in active state plotted against that by the same stimulus in quiescence for the cell shown in **a**. The best-fit linear regression line is shown. (**c**) Normalized PSTHs for all the tone responses in two states for the cell shown in **a**. Arrows indicate response onsets. Δt is the onset difference. (**d**–**f**) TRFs of a L4 cell. Data are presented as in **a**–**c**. (**g**) Distribution of correlation coefficients (r) for all the recorded L2/3 cells. (**h**) Distribution of slopes of the linear regression (that is, the gain value). Arrow points to the mean value. (**i**) Distribution of differences in onset latency (A – Q) of spike responses. (**j**) CF of spike TRF in the A versus Q state. The best-fit linear regression line is shown. (**k**) Bandwidth at 20 dB above the intensity threshold (BW20) of spike TRF in the A versus Q state. (**l**) Intensity threshold of spike TRF in the A versus Q state. (**m**–**r**) Summary for L4 cells. Data are presented as in **g**–**l**.

(spontaneous: 2.29 ± 0.89 Hz for anesthesia, 4.06 ± 1.1 Hz for awake, $P < 0.05$, t test; evoked: 50.2 ± 12.7 Hz for anesthesia, 60.2 ± 11.7 Hz for awake, $P < 0.05$, t test; $n = 55$ and 32 neurons for anesthesia and awake states, respectively).

Behavioral state–dependent gain modulation

To determine the nature of the behavioral state–dependent modulation of auditory processing, we continuously mapped the frequency-intensity tonal receptive field (TRF) of spiking response in an individual cell by applying tone pips of different frequencies and intensities (Online Methods). Trials during active (A) states were separated from those in quiescence. Given that the A – L state produced similar effects as locomotion (**Fig. 1n**,**q**), we did not further separate the trials in these two states. The spike TRF was reconstructed from at least ten complete sets of spike responses to 41 testing frequencies and eight testing intensities. In an example L2/3 cell, the A state apparently reduced the firing rates without affecting the overall shape of the spike TRF (**Fig. 2a**). In the TRF, the average evoked spike number in an A-state trial strongly correlated with that in the corresponding Q-state trial (Pearson's correlation coefficient, $r = 0.94$; **Fig. 2b**), indicating that firing rates to different tone stimuli were reduced in proportion. In other words, firing rates were scaled down. The slope of the linear regression line (0.71) indicated an ~30% reduction in response gain (**Fig. 2b**). Concurrently, the onset of the evoked spike response was slightly delayed in the A state compared with in the Q state (**Fig. 2c**), and there was a reduced level of spontaneous activity. In comparison, in the example L4 cell, the A state did not apparently affect evoked or spontaneous firing rates or the shape of the TRF (**Fig. 2d**–**f**), with the slope of the linear regression line being close to 1 (0.98; **Fig. 2e**). In addition, the onset delay of the evoked spike response was not apparently changed (**Fig. 2f**).

In all of the 17 recorded L2/3 excitatory cells, the evoked spike rate in the Q state correlated well with that in the A state (**Fig. 2g**). The slopes of the linear regression line for A-state versus Q-state responses were nearly all below 1 (mean ± s.d., 0.77 ± 0.14; **Fig. 2h**). This indicates that the response gain of L2/3 excitatory cells was reduced in active states. Most of these cells showed a 1–2-ms (1.5 ± 0.7 ms, mean ± s.d.) delay of spiking response onset in the A state relative to the Q state (**Fig. 2i**). In ten of these cells, we obtained complete TRFs for both the A and Q states. For these TRFs, no apparent

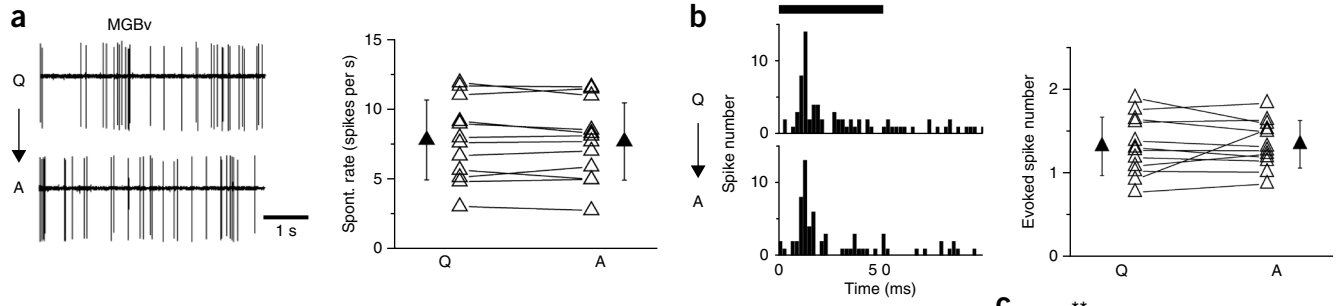

Figure 3 Activity of thalamic neurons and summary of SNR under different behavioral states. (**a**) Left, sample records of spontaneous spikes in an MGBv neuron in the Q and A states. Right, summary of average spontaneous firing rates ($N = 12$ cells). Data points from the same cell are connected with a line. Solid symbol represents mean ± s.d. (paired t test, $P = 0.4795$, $t = 0.7320$, $n = 12$ cells). (**b**) Left, PSTH for CF tone–evoked spikes in different states in the same MGBv neuron as shown in **a**. Right, summary of average evoked spike numbers by CF tones in different states (paired t test, $P = 0.7640$, $t = -0.3078$, $n = 12$ cells). (**c**) SNR in the A relative to Q state. There was a significant increase in L2/3 cells. From left to right, Wilcoxon signed rank test (**$P = 0.0017$, $Z = 3.435$), t test ($P = 0.5834$, $t = 0.5614$), t test ($P = 0.6282$, $t = 0.4982$). Error bars represent s.d. in all panels.

difference was observed for the characteristic frequency (**Fig. 2j**), the bandwidth at 20 dB above the intensity threshold (BW20; **Fig. 2k**) or the intensity threshold of TRF (**Fig. 2l**) between the two different states, indicating that the shape and sharpness of TRF remained the same despite the change in response gain. We found no correlation between the scaling factor and the cortical depth of recorded L2/3 cells (**Supplementary Fig. 3**). In comparison, in all of the 15 recorded L4 cells, the slopes were close to 1 (1.02 ± 0.09, mean ± s.d.), indicating no change in response gain (**Fig. 2m**,**n**). The onset latency of evoked spiking response was overall unaffected by changes of behavioral state (Δlatency = 0.1 ± 0.8 ms; **Fig. 2o**) and the shape of spike TRF was unchanged (**Fig. 2p**–**r**).

The absence of response changes in L4 suggests that activity of auditory thalamic neurons may not change during active behaviors. To confirm this, we performed loose-patch recordings in the ventral part of the medial geniculate body (MGBv), the thalamic nucleus that provides direct feedforward input into A1. Indeed, neither the spontaneous (**Fig. 3a**) nor the evoked spike responses of thalamic

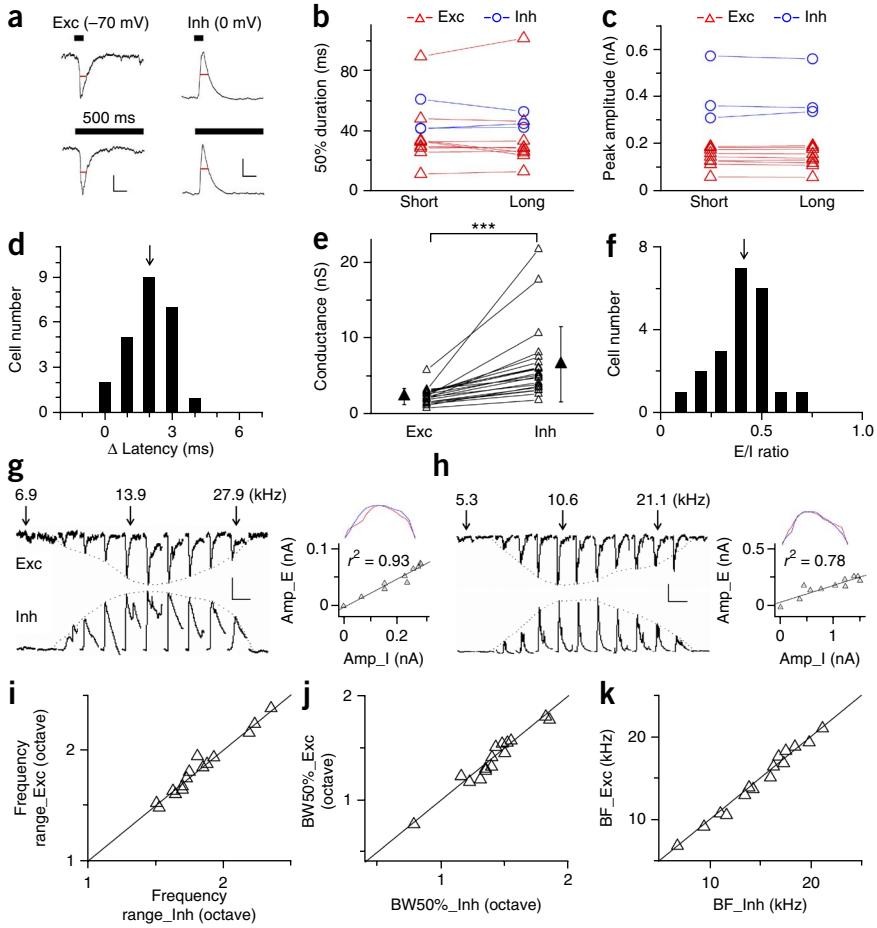

Figure 4 Properties of synaptic responses in quiescence. (**a**) Average traces of excitatory and inhibitory currents evoked by a BF tone at 40 dB SPL in an example pyramidal neuron. Black line indicates tone duration. Red line marks 50% duration of the current. Scale bars represent 50 (exc) /100 (inh) pA and 100 ms. (**b**) Durations of BF tone–evoked synaptic currents. Short, 50 ms; long, 200 or 500 ms. Wilcoxon signed-rank test ($P = 0.81$, 0.73; $Z = 0.2439$, 0.4024; $N = 9$, 3 for exc and inh, respectively). (**c**) Comparison of peak amplitudes (paired t test, $P = 0.4$, 0.89; $t = 0.8876$, 0.1520; $N = 9$, 3 for exc and inh, respectively). (**d**) Differences in excitatory and inhibitory onset latency (Inh – Exc). Arrow points to the mean value. (**e**) Comparison of peak amplitudes. Wilcoxon signed-rank test, ***$P = 0.0001$, $Z = -4.464$, $n = 21$. Error bars represent s.d. (**f**) Distribution of E/I ratios of peak conductances. (**g**) Frequency tuning of excitation and inhibition in an example cell. Left, average excitatory and inhibitory currents to tones at different frequencies (interval, 0.2 octaves). Scale bars represent 30 (exc) / 100 (inh) pA and 200 ms. Right, peak amplitude of excitatory versus inhibitory current evoked by the same stimulus. Top inset, superimposed normalized frequency tuning curves for excitation (red) and inhibition (blue). (**h**) Another example cell plotted as in **g**. Scale bars represent 100 (exc) / 500 (inh) pA and 200 ms. (**i**–**k**) Comparison of frequency range (**i**), half-peak bandwidth (**j**) and BF (**k**) between excitation and inhibition in the same cell ($P = 0.52$, 0.56, 0.46, respectively; paired t test, $n = 15$ cells). The unity line is shown.

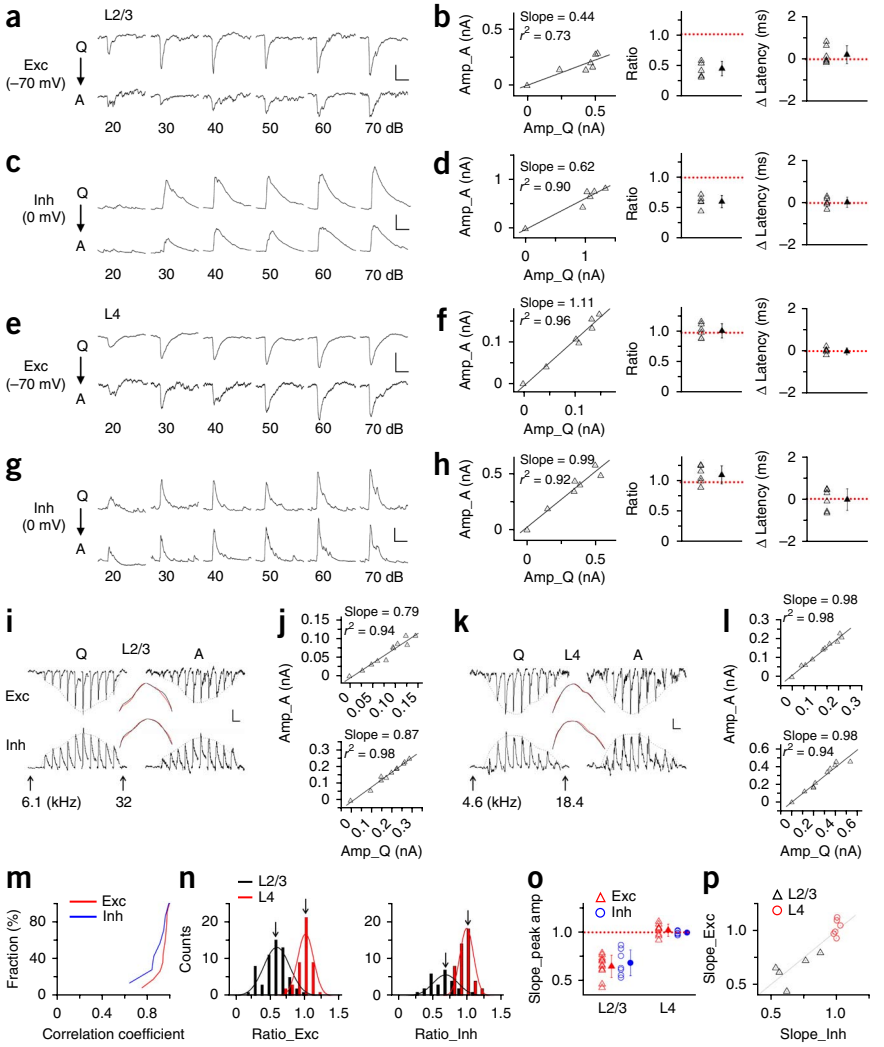

Figure 5 Modulation of synaptic responses by behavioral state. (**a**) Average evoked excitatory currents to BF tones at different intensities in quiescence and active states in a L2/3 excitatory cell. Scale bars represent 200 pA and 100 ms. (**b**) Left, peak excitatory amplitudes in active versus quiescence state with the best-fit line shown. The near zero point depicts the responses to 10-dB tones not shown in **a**. Middle, ratio of response amplitudes (Q/A) for all testing intensities (zero responses excluded). Solid symbol represents mean ± s.d. Right, difference in onset latency of evoked synaptic currents (A – Q). (**c**,**d**) Inhibitory responses in "Q" and "A" states recorded in the same L2/3 neuron. Scale bars represent 500 pA and 100 ms. (**e**–**h**) Excitatory and inhibitory responses of a L4 excitatory cell. Scale bars represent 100 pA and 100 ms (**e**), and 200 pA and 100 ms (**g**). (**i**) Excitatory and inhibitory currents to tones of different frequencies in a L2/3 cell. Scale bars represent 40 (exc) / 80 (inh) pA and 200 ms. Inset, superimposed normalized excitatory (top) and inhibitory (bottom) frequency tuning curves in quiescence (black) and active (red) states. (**j**) Peak response amplitude in active versus quiescence state for the cell shown in **i**. Top, excitation; bottom, inhibition. (**k**,**l**) An example L4 cell plotted in the same manner as in **i**,**j**. Scale bars represent 50 (exc) / 150 (inh) pA and 200 ms. (**m**) Cumulative distribution of correlation coefficients for synaptic responses in the A versus Q state for L2/3 neurons. (**n**) Distribution of ratios between peak synaptic amplitudes in the A and Q states (A/Q) for all tone stimuli in all recorded cells. Arrows indicate mean values. Left, excitation; right, inhibition. (**o**) Slopes (scaling factors) of the linear regression for the A versus Q peak synaptic responses in all recorded cells. No significant difference between scaling factors of excitation and inhibition in L2/3 cells ($P = 0.5481$, $t = 0.6136$, unpaired t test, $n = 11, 7$ for excitatory and inhibitory, respectively). (**p**) The scaling factors for excitatory responses plotted against that for inhibitory responses in the same cell. For L2/3, $P = 0.6177$, $t = 0.5402$, paired t test, $n = 5$. Error bars represent s.d. in all panels.

neurons (**Fig. 3b**) changed substantially from the Q to A state, indicating that auditory thalamic neurons were not directly affected by the behavioral changes.

Although the evoked firing rate of L2/3 cells was reduced in active states, their spontaneous activity was even more suppressed, and the signal-to-noise ratio (SNR), as defined by the ratio of the evoked firing rate to the spontaneous firing rate, was increased (**Fig. 3c**). This increased SNR, together with the unchanged intensity threshold (**Fig. 2l**), indicates that the sensitivity of auditory processing was not reduced in active states despite the decreased response level.

Balanced excitation and inhibition in quiescent state

The properties of sound-driven synaptic excitation and inhibition to auditory cortical neurons in the awake brain remain unknown, as previous studies have been mostly carried out in anesthetized preparations[2,20–23]. To understand the synaptic mechanisms underlying the observed behavioral state–dependent modulation of response gain, we performed whole-cell voltage-clamp recordings to reveal excitatory and inhibitory synaptic inputs to A1 neurons (Online Methods). We first examined the properties of synaptic responses in quiescence. As shown by an example cell, a best-frequency (BF) tone elicited robust excitatory and inhibitory currents in the same cell (**Fig. 4a**). The major component of these currents could be best described as transient, as its temporal duration, as measured at the half-peak level (that is, 50% duration), did not increase with increasing tone durations (**Fig. 4b**). In addition, the peak amplitude of synaptic currents did not increase with increasing stimulus durations (**Fig. 4c**). The onset latency of inhibitory current was mostly delayed by 1–3 ms (1.95 ± 1.03 ms, mean ± s.d.) relative to that of the excitatory current evoked by the same stimulus (**Fig. 4d**), similar to what has been observed in anesthetized animals[20–23,26], and suggesting that the inhibition has a fast feedforward nature[2,27]. The amplitude of inhibitory conductance was larger than that of the corresponding excitatory conductance (**Fig. 4e**), with a mean excitatory to inhibitory (E/I) ratio of 0.42 ± 0.12 (**Fig. 4f**), which is consistent with our previous studies in anesthetized animals[23,26,28,29]. We further compared the frequency tuning of excitation and inhibition at a moderate intensity level (40–50-dB sound pressure level, SPL). As shown by two example cells (**Fig. 4g**,**h**), the total frequency ranges for evoked excitatory and inhibitory currents were about the same, and the amplitude of excitatory current was linearly correlated with that of the inhibitory current evoked by the same stimulus, resulting in very similar excitatory and inhibitory frequency tuning curves (**Fig. 4g**,**h**). This finding suggests a functional balance of excitation and inhibition, that is, the strength of inhibition covaries

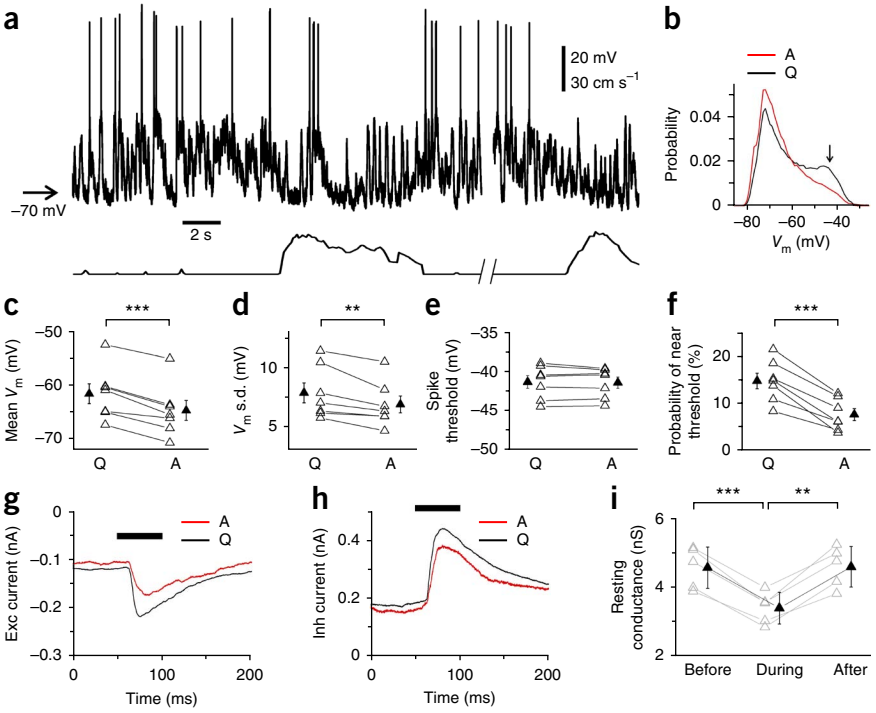

Figure 6 Modulation of resting membrane potential and resting conductance by behavioral state. (**a**) Sample current-clamp recording records (top) together with the simultaneously recorded speeds (bottom) for an example L2/3 neuron. Arrow labels the level for −70 mV. (**b**) Normalized distribution of membrane voltages during quiescent and active states for the cell shown in **a**. Arrow points to the average spike threshold of the cell. (**c**–**f**) Comparison of mean resting membrane potential (**c**), s.d. of resting V_m (**d**), spike threshold (**e**) and percentage of V_m values near spike threshold (not lower than the threshold by more than 10 mV; **f**) under different behavioral states for seven recorded L2/3 neurons. Error bars represent s.e.m., paired *t* test ($P = 0.0002$, $P = 0.0083$, $P = 0.5496$, $P = 0.0002$; $t = 8.114$, 3.862, 0.6338, 8.139 for **c**–**f**, respectively). (**g**) Average excitatory currents of an example cell in response to BF tones (70 dB SPL) in different states. Thick black line marks tone duration. (**h**) Average inhibitory currents of the same cell. (**i**) Resting conductances right before, during and after an epoch of active behaviors for five L2/3 cells. Data points from the same cell are connected by lines. Error bars represent s.d. $N = 5$, paired *t* test ($P = 0.0004$, $P = 0.0015$; $t = 10.65$, − 7.810). $^{**}P < 0.01$, $^{***}P < 0.001$.

with that of excitation. In a total of 15 recorded cells, we observed that the frequency range of excitation was not different from that of inhibition (**Fig. 4i**). The bandwidth of excitatory frequency tuning curve, as measured at the half-peak level (BW50%), was not different from that of the inhibitory tuning curve of the same cell (**Fig. 4j**). Excitatory and inhibitory tuning curves also exhibited the same best frequency (**Fig. 4k**). Together, these results indicate that, in awake A1, excitation and inhibition are balanced in the frequency domain, with inhibition being briefly temporally delayed relative to excitation.

Scaling down of excitation and inhibition in active states

To examine how behavioral state regulates synaptic inputs, we applied best-frequency tones and varied their intensity in a random order. Responses were parsed into active state (including locomotion) and quiescence trials. As shown by an example L2/3 excitatory cell, the average excitatory current in response to BF tones increased in amplitude with increasing tone intensities (**Fig. 5a**). In the A state, the excitatory currents to all tone intensities became smaller (**Fig. 5a**) in an approximately proportional manner (**Fig. 5b**). The onset latencies of evoked excitatory currents were not changed apparently (**Fig. 5b**). The evoked inhibitory currents to different tone intensities were also reduced by a similar factor from the Q to A state, whereas the timing of inhibitory currents was not affected (**Fig. 5c**,**d**). In comparison, in a L4 excitatory cell, neither the excitatory nor inhibitory currents changed apparently in their amplitudes, and the onset latencies of these currents were unaffected (**Fig. 5e**–**h**).

To examine state-dependent changes of synaptic responses in the frequency domain, we applied tone stimuli of different frequencies at a moderate intensity (40 or 50 dB SPL). As shown by an example L2/3 excitatory cell (**Fig. 5i**), tone-evoked excitatory and inhibitory currents were both reduced in amplitude from the Q to A state. The strong linear relationship between synaptic responses in the two states suggests a scaling of both excitatory and inhibitory inputs (**Fig. 5j**). Such coordinated modulation resulted in apparently unchanged frequency tuning of synaptic inputs, as demonstrated by the superimposed normalized synaptic tuning curves for A and Q states (**Fig. 5i**). Consistent with the results of spiking response, in L4, we did not observe apparent effects of the A state on the amplitude of either evoked excitatory or inhibitory synaptic responses (**Fig. 5k**,**l**). Together, these results suggest that tone-evoked excitatory and inhibitory inputs to L2/3 cells are scaled down in behaviorally active states, thereby preserving the functional balance between excitation and inhibition.

In all of the 13 recorded L2/3 cells, we observed a strong linear correlation between evoked synaptic amplitudes in the A and Q states for both excitation and inhibition (**Fig. 5m**), further demonstrating a scaling of excitatory and inhibitory responses by changes of behavior state. To determine the scaling factor, we calculated the ratio of peak response amplitude in the A versus the Q state for each tone-evoked response. As shown by the distribution of ratios for all the recorded neurons (**Fig. 5n**), the scaling factors were nearly all lower than 1 for both excitation and inhibition in L2/3 (mean ± s.d.; excitation, 0.64 ± 0.18; inhibition, 0.70 ± 0.18). In contrast, in L4, the scaling factors were 1.03 ± 0.11 and 1.01 ± 0.10 for excitation and inhibition, respectively (**Fig. 5n**). We also quantified the scaling factor by the slope of the linear regression for peak response amplitudes in the A versus the Q state (**Fig. 5o**). The average slope was 0.65 ± 0.11 for excitation and 0.69 ± 0.13 for inhibition in L2/3 cells, and 1.02 ± 0.06 and 1.00 ± 0.02, respectively, in L4 cells (**Fig. 5o**). Similar results were obtained when the charge transfer of synaptic currents was measured (**Supplementary Fig. 4**). When examined in the same cell, the slope for excitatory responses was similar to that for inhibitory responses (**Fig. 5p**). Thus, evoked excitation and inhibition in a L2/3 cell were reduced by a similar factor from the Q to A state, whereas excitation and inhibition in a L4 cell were not affected by changes of behavioral state (**Fig. 5o**). Finally, we argued that the reduction in recorded synaptic responses was not a result of compromised recording quality during animal movements, as the linear current-voltage relationship of the cell remained as good in active states (**Supplementary Fig. 5**) and there was no obvious change in series resistance with

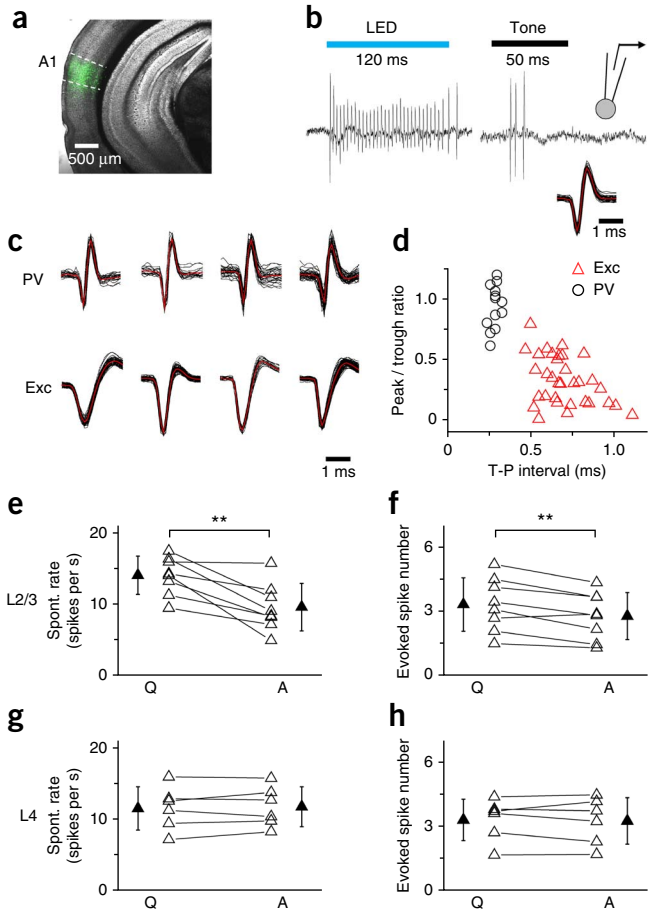

Figure 7 Changes of activity of PV neurons between different behavioral states. (**a**) Confocal image of a brain section showing ChR2-EYFP expression in the A1 region. (**b**) Left, sample loose-patch recording trace showing a train of evoked spikes of a PV cell to blue LED illumination (marked by the blue bar). Right, sample spike response of the same cell to CF-tone stimulation. Top inset, schematic drawing of loose-patch of a cell. Bottom inset, superimposed 500 individual spikes (black) and the average spike shape (red) of the cell. (**c**) Spike shapes of four more PV and excitatory cells. (**d**) Plot of peak-to-trough amplitude ratio versus trough-to-peak (T-P) interval for average spike shapes of PV and excitatory cells recorded with loose-patch methods. Optogenetically identified PV cells were labeled by open circles. (**e**) Summary of spontaneous firing rates of recorded L2/3 PV cells in different states. $N = 8$ cells. $^{**}P = 0.0044$, $t = 4.140$, paired t test. (**f**) CF tone–evoked spike numbers for the cells in **e**. $^{**}P = 0.0047$, $t = 4.086$, paired t test. (**g**) Summary of spontaneous firing rates for PV cells recorded in L4. $P = 0.5013$, $t = -0.7243$, paired t test, $n = 6$ cells. (**h**) CF tone–evoked spike numbers for the cells in **g**. $P = 0.7286$, $t = 0.3671$, paired t test. Error bars represent s.d. in all panels.

animal movements (**Supplementary Fig. 6**). In addition, we found that the response amplitude to the same stimulus remained essentially unchanged before and after an epoch of animal movements and remained relatively stable from the start until the end of the recording sessions (**Supplementary Fig. 7**).

Change of membrane properties in active states

In visual cortex, locomotion is shown to cause a depolarization of neuronal membrane potential, which contributes to the increased visual responses[18,19]. The reduced auditory responses that we observed suggest that the neuron's membrane potential might be hyperpolarized instead. We therefore recorded resting membrane potentials in current-clamp mode using a K^+-based internal solution (Online Methods) from L2/3 excitatory neurons. In the absence of sound stimulation, the membrane potential (V_m) fluctuated largely with occasional appearance of spontaneous spikes (**Fig. 6a**), but the distribution of potentials was statistically unimodal ($P > 0.05$, Hartigan's dip test; **Fig. 6b**). In active states, the distribution shifted toward more hyperpolarized values (**Fig. 6b**), resulting in a more hyperpolarized mean V_m. In all similarly recorded cells ($n = 7$), the distribution of potentials was unimodal in both states, and the transition from the Q to A state resulted in a more hyperpolarized mean V_m (from −61.67 ± 1.83 mV to −64.75 ± 1.84 mV; **Fig. 6c**), as well as a reduction of V_m variability (**Fig. 6d**). The level of spike threshold remained constant (**Fig. 6e**). As a consequence, the probability of instantaneous V_m being within 10 mV of the spike threshold was reduced in the A compared with the Q state (**Fig. 6f**). This can contribute to the reduction of both spontaneous and evoked spiking activity of L2/3 neurons. In addition, we found a reduction of baseline conductance from the Q to A state (**Fig. 6g–i**), which would result in an increase of input resistance of the cell. The decrease of baseline conductance may be partly attributed to reduced spontaneous synaptic events, as evidenced by the reduction of spontaneous spiking activity of L2/3 neurons (**Fig. 1i**).

Modulation of PV neuron activity

The reduced auditory evoked inhibition to L2/3 neurons in active states likely reflects reduced inhibitory neuron activity. It is known that the major source of inhibition to L2/3 excitatory cells comes from the same layer[30]. Given that parvalbumin (PV)-expressing neurons most likely contribute to the feedforward inhibition in L2/3 excitatory cells[24] and have a major role in controlling the network gain as a result of their high firing rates and strong synaptic connections[24,31], we specifically examined PV neuron activity in different behavioral states. By injecting an adeno-associated virus (AAV) viral vector encoding Cre-dependent channelrhodopsin2 (ChR2) in PV-Cre mice in which Cre recombinase is specifically expressed in PV cells (**Fig. 7a** and Online Methods), we were able to identify PV neurons with a previously described optogenetic method[32]. With loose-patch recordings, we actively searched for PV neurons, the identification of which was based on their trains of spikes in response to a pulse of blue LED light applied to the A1 surface (**Fig. 7b**). These neurons responded robustly to tone stimuli (**Fig. 7b**). Consistent with previous reports using two-photon imaging guided loose-patch recordings[24,33], PV neurons exhibited shorter trough-to-peak intervals in their spike shapes than excitatory neurons (**Fig. 7c**,**d**). They also tended to have higher peak-to-trough amplitude ratios than excitatory cells (**Fig. 7d**). In L2/3, we found that both the spontaneous and evoked spiking activity of PV neurons was reduced from the Q to A state (**Fig. 7e**,**f**), whereas PV cell activity was not affected in L4 (**Fig. 7g**,**h**). These results suggest that the L2/3 networks comprising both excitatory and PV inhibitory neurons are generally suppressed by active behaviors.

Contribution of L1-mediated suppression

It has been shown previously that L1 is involved in modulating activity in L2/3 (refs. 17,34). We then examined whether L1, which contains only inhibitory neurons[35,36], is involved in the behavioral state–dependent modulation of L2/3 activity. With loose-patch recordings, we found that L1 neurons were modulated by behavioral state differently from L2/3 and L4 cells: their spontaneous (**Fig. 8a**) and evoked (**Fig. 8b**) firing rates were both increased rather than decreased from the Q to A state. Given that L1 neurons inhibit both excitatory and inhibitory cells in L2/3 (refs. 34,37,38), the increased activity of L1

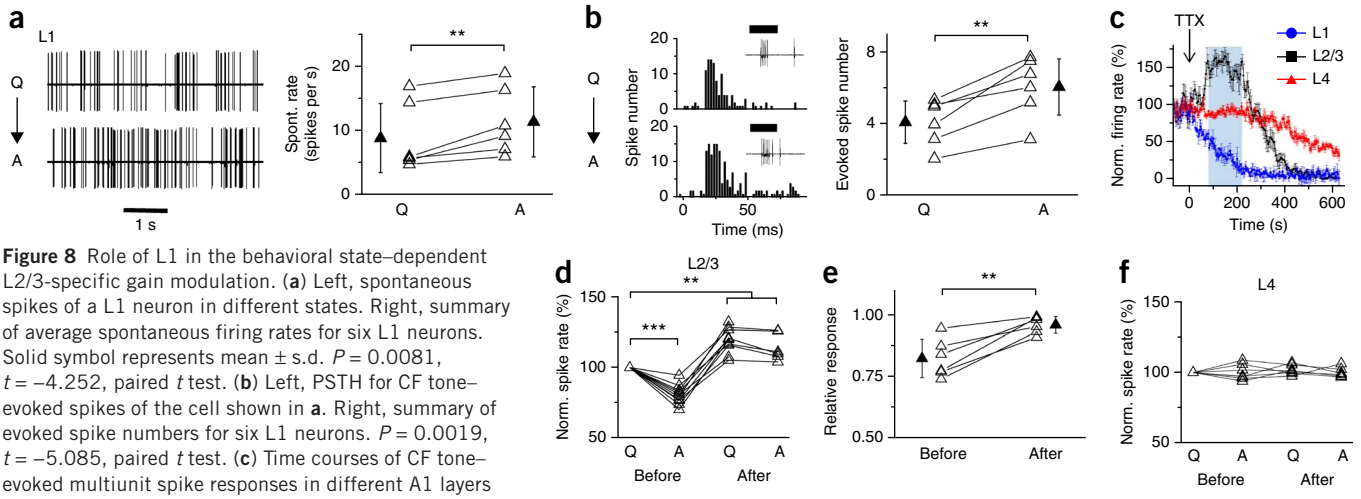

Figure 8 Role of L1 in the behavioral state–dependent L2/3-specific gain modulation. (**a**) Left, spontaneous spikes of a L1 neuron in different states. Right, summary of average spontaneous firing rates for six L1 neurons. Solid symbol represents mean ± s.d. $P = 0.0081$, $t = -4.252$, paired t test. (**b**) Left, PSTH for CF tone–evoked spikes of the cell shown in **a**. Right, summary of evoked spike numbers for six L1 neurons. $P = 0.0019$, $t = -5.085$, paired t test. (**c**) Time courses of CF tone–evoked multiunit spike responses in different A1 layers after the topical application of TTX (at time zero). Shaded area denotes the analysis time window during which L2/3 responses were increased to a stable level, whereas L4 responses remained unaffected. $N = 4$ animals for each layer. (**d**) Summary of evoked firing rates of individual L2/3 excitatory cells in different behavioral states before and after TTX application. Spike rates were normalized by "Q" state before TTX application. $N = 10$ cells. Among these ten cells, six were also recorded in active states after TTX application. (**e**) Summary of relative response levels (A/Q) before and after TTX application. $P = 0.0035$, $t = -5.193$, paired t test, $n = 6$. (**f**) Summary of normalized evoked spike numbers in different states before and after TTX application for L4 neurons. $N = 6$ cells. $^{**}P < 0.01$, $^{***}P < 0.001$, paired t test. Error bars represent s.d. in all panels.

neurons may generally increase the inhibitory tone in the L2/3 network, leading to the observed reduced activity of L2/3 cells. To further confirm the involvement of L1, we silenced L1 spiking by applying 5 μM tetrodotoxin (TTX) to the A1 surface, following a previously published method[37]. We monitored auditory-evoked multiunit spike responses in different layers before and after TTX application. In a limited time window (~150 s) after the topical application of TTX, the firing rate of L1 neurons was gradually reduced to zero (**Fig. 8c**). Concurrently, the evoked firing rate of L2/3 neurons increased to a stable level, whereas that of L4 neurons remained unchanged. These results indicate that L1 spiking activity tonically suppressed L2/3, but not L4, neurons so that removing L1 inhibition increased the firing rates of L2/3 cells. Beyond the time window, firing rates in L2/3 were gradually reduced, indicating that L2/3 cells were also progressively affected by TTX. L4 neurons also progressively reduced their firing rates, but with a delay. Thus, the 150-s window provided a good opportunity to examine the effect of silencing L1 spikes while leaving spikes in L2/3 and L4 unaffected by the drug. We next examined CF tone–evoked spikes in individual neurons with loose-patch recordings. Before TTX application, the L2/3 cells exhibited a normal reduction of response level from the Q to A state (20.1 ± 6.9%; **Fig. 8d**,**e**). In the 150-s window after the drug application, the response level in the Q state was increased by 19.2 ± 8.6% compared with that before the drug application (**Fig. 8d**). From the Q to A state, response level was reduced by only 4.1 ± 3.4%. Thus, the behavioral state–dependent gain reduction was largely blocked when L1 spiking was silenced, supporting the notion that the increase of L1 firing rates in active states was responsible, at least partially, for the reduced response level in L2/3. As a control, the response level of L4 neurons was not affected by the drug application in the analysis time window or by the change of behavioral state (**Fig. 8f**), which is consistent with our earlier observations.

DISCUSSION

How sensory processing in cerebral cortex is modulated by behavioral and cognitive states has been an important question for understanding the integrative function of the brain. To address this question, it is critical to examine how sensory-evoked responses in individual cortical neurons are modulated at cellular and synaptic levels. Using high-quality *in vivo* whole-cell voltage-clamp recordings, we detected excitatory and inhibitory synaptic inputs to a cortical neuron under different behavioral states. Our results suggest a robust functional balance between synaptic excitation and inhibition in the awake A1, as manifested by the covariation of inhibitory and excitatory response amplitudes across different tone frequencies. Relative to quiescence, behaviorally active states scaled down excitatory and inhibitory inputs at a similar level in L2/3, but not L4, neurons, resulting in a proportional reduction of their spike responses to different tone stimuli. As a consequence, the sensory tuning of spike response, as well as the functional balance between excitation and inhibition, was preserved.

Behavioral state–dependent gain modulation

The observed suppression of auditory responses during active behaviors is reminiscent of a previous report that the animal's engagements in an auditory task result in reduced auditory cortical responses[10]. In the current study, the magnitude of the modulation is relatively small. The average effect on evoked spike responses is about 20% (**Fig. 1o**), whereas it can be as high as 50% for some individual neurons. Nevertheless, the moderate modulation effect may possibly change the information transfer in the A1 and consequently affect sound-dependent behaviors. This notion is supported by a study in the visual cortex showing that a moderate reduction in evoked firing rates caused by optogenetically activating PV inhibitory neurons can lead to a substantial change in performance in visual detection tasks[39]. Our results contrast with observations in visual and somatosensory cortices that behaviorally active states depolarize the membrane potential of cortical neurons[16–19], and with the idea that active states are characterized by an increase in excitatory and inhibitory conductances, even in baseline conditions without sensory stimuli[40]. It is possible that the modulatory effect of behavioral state is specific to sensory modality. Or it may depend on whether the specific sensory processing is engaged in the behavior that provides the modulation. Possibly during locomotion and whisking, the animal's exploration of the external environment depends more on visual and tactile than on auditory perception. In accordance with this change in task demands, the relative salience of auditory information may be reduced.

Despite the reduction of response level, there was no change in the shape or size of TRFs of L2/3 neurons from quiescence to active states. And the intensity threshold and frequency tuning were well preserved. This is a result of gain modulation of spike responses, that is, responses to different tone stimuli are scaled by a similar factor. Counter-intuitively, the SNR of auditory information in this output layer (L2/3) of A1 was in fact increased by about 35% in active states (**Fig. 3c**). The enhanced SNR is a result of relatively more suppressed spontaneous activity than of evoked activity, which is different from the observations in visual cortex that locomotion elevates SNR by enhancing sensory-evoked responses[18,19], resulting in enhanced visual discrimination[19]. Although the functional relevance of this enhanced SNR in A1 remains to be examined with behavioral studies, our results suggest that the sensitivity, as well as the quality, of auditory processing is at least maintained from quiescence to active states.

Balanced excitation and inhibition in awake cortex

Spectrotemporally balanced excitation and inhibition has been demonstrated in auditory cortical neurons of anesthetized animals, characterized by a similar frequency tuning of excitation and inhibition, a roughly constant ratio between excitatory and inhibitory response amplitudes across different stimuli, and a stereotypic temporal sequence of excitation briefly followed by inhibition[20–23]. The short interval (~2–3 ms) between the onsets of excitation and inhibition is consistent with a synaptic circuit dominant with feedforward inhibition[2,20,22]. Recently, an awake recording study in the visual cortex found that, although balanced excitation and inhibition is prevalent in the anesthetized cortex, inhibition is much more broadly tuned than excitation in terms of spatial tuning in the awake cortex[41]. Our study in the auditory cortex, however, indicates that the functional balance between excitation and inhibition is ubiquitous across different brain states and that this balance is actively preserved through a specific modulation of excitation and inhibition. The evoked synaptic excitation and inhibition are reduced by a similar factor from quiescence to active states. Such balanced scaling down of excitatory and inhibitory inputs would result in reduced output responses[42,43], as well as a longer integration time for spike generation[27] (**Fig. 2i**). In addition, the scaled excitatory and inhibitory inputs indicate that the observed gain modulation of spike responses could be largely attributed to a network effect of suppression of L2/3 circuits, which results in a reduction of total evoked synaptic conductance. Together, our results strongly suggest that balanced excitation and inhibition is a fundamental synaptic circuit basis for auditory cortical processing in awake conditions.

L1-mediated suppression of L2/3 activity

Modulation of cortical activity may be carried out by bottom-up or top-down pathways[44]. It has been shown in mice that action potential firing in the somatosensory thalamus increases during whisking, which drives the desynchronized state in the somatosensory cortex[45]. The absence of changes in spiking responses in L4 and MGBv neurons, as well as in synaptic inputs to L4 cells, that we observed argues that the behavioral state–dependent suppression of sensory responses in L2/3 of A1 is unlikely to be a result of a modulation of neuronal activity in subcortical nuclei along the ascending auditory pathway. On the other hand, previous studies have suggested that behavior can affect network state via corticocortical inputs[17,46]. Corticocortical projections are known to ramify their axons in L1 (refs. 47–50), which is in a good position to mediate state-dependent modulation of cortical activity in a top-down control. We found that L1 activity was increased from quiescence to active states. Given that L1 activity can inhibit both excitatory and inhibitory cells in L2/3 (refs. 34,37,38), the increased spiking of L1 neurons may generally enhance the inhibitory tone in the L2/3 network. This was evidenced by the increase of spike responses of L2/3 excitatory cells when spiking of L1 neurons was suppressed. Silencing of L1 spiking activity largely blocked the reduction of sensory-evoked responses of L2/3 neurons when animals transitioned from quiescence to active states. This result indicates that the behavioral state–dependent gain modulation in the L2/3 network can be attributed, at least partially, to a direct regulation of L1-mediated inhibition.

Another possible way of modulating cortical activity is through neuromodulatory systems. In the mouse cortex, neuromodulatory projections such as cholinergic and noradrenergic fibers are distributed diffusely in all cortical layers without clear patterns (see the Allen Brain Atlas data portal at http://www.brain-map.org). In the visual cortex, the locomotion-induced depolarization of membrane potential and increase of firing rate is attributed to an effect of noradrenergic input and is more or less uniform across L2/3 and L4 (ref. 18), which is consistent with the diffuse pattern of noradrenergic fibers. We observed the suppression of spontaneous and evoked responses induced by active behaviors in L2/3, but not in L4. To the best of our knowledge, there have been no reports about lamina-specific expression patterns of receptors for neuromodulators that are consistent with our observations. Nevertheless, our results do not exclude the possibility that the observed activity changes, including the enhancement of L1 activity, are mediated by the effects of specific neuromodulators.

In summary, we found that a balanced scaling down of excitatory and inhibitory inputs underlies the suppressive gain modulation of sensory responses of L2/3 excitatory neurons induced by active behaviors. We postulate that scaling of synaptic inputs may be a simple strategy employed by brain circuits to maintain the quality of sensory processing while optimizing the level of salience of sensory information according to momentary behavioral demands.

METHODS

Methods and any associated references are available in the online version of the paper.

Note: Any Supplementary Information and Source Data files are available in the online version of the paper.

ACKNOWLEDGMENTS

We thank B. Zingg and L.Y. Li for the help on viral injection and Nissl staining. This work was supported by grants to L.I.Z. from the US National Institutes of Health (R01DC008983) and the David and Lucile Packard Foundation (Packard Fellowships for Science and Engineering). H.W.T. was supported by US National Institutes of Health grant R01EY019049. Z.X., L.I.Z. and F.L. were supported by grants from the National Natural Science Foundation of China (U1301225, 31228013, 31200831) and a 973 program (2014CB943002).

AUTHOR CONTRIBUTIONS

L.I.Z., Z.X. and H.W.T. conceived and supervised the study. M.Z. and F.L. performed all of the experiments. L.L., H.L. and X.R.X. contributed to data collection. M.Z., F.L., H.W.T. and L.I.Z. performed data analysis. H.W.T. and L.I.Z. wrote the manuscript.

COMPETING FINANCIAL INTERESTS

The authors declare no competing financial interests.

1. Oswald, A.M., Schiff, M.L. & Reyes, A.D. Synaptic mechanisms underlying auditory processing. *Curr. Opin. Neurobiol.* **16**, 371–376 (2006).
2. Wu, G.K., Tao, H.W. & Zhang, L.I. From elementary synaptic circuits to information processing in primary auditory cortex. *Neurosci. Biobehav. Rev.* **35**, 2094–2104 (2011).
3. Petersen, C.C. & Crochet, S. Synaptic computation and sensory processing in neocortical layer 2/3. *Neuron* **78**, 28–48 (2013).

4. Callaway, E.M. Local circuits in primary visual cortex of the macaque monkey. *Annu. Rev. Neurosci.* **21**, 47–74 (1998).
5. Douglas, R.J. & Martin, K.A. Neuronal circuits of the neocortex. *Annu. Rev. Neurosci.* **27**, 419–451 (2004).
6. Fanselow, E.E. & Nicolelis, M.A. Behavioral modulation of tactile responses in the rat somatosensory system. *J. Neurosci.* **19**, 7603–7616 (1999).
7. Reynolds, J.H. & Chelazzi, L. Attentional modulation of visual processing. *Annu. Rev. Neurosci.* **27**, 611–647 (2004).
8. Ferezou, I. *et al.* Spatiotemporal dynamics of cortical sensorimotor integration in behaving mice. *Neuron* **56**, 907–923 (2007).
9. Lee, S., Carvell, G.E. & Simons, D.J. Motor modulation of afferent somatosensory circuits. *Nat. Neurosci.* **11**, 1430–1438 (2008).
10. Otazu, G.H., Tai, L.H., Yang, Y. & Zador, A.M. Engaging in an auditory task suppresses responses in auditory cortex. *Nat. Neurosci.* **12**, 646–654 (2009).
11. Niell, C.M. & Stryker, M.P. Modulation of visual responses by behavioral state in mouse visual cortex. *Neuron* **65**, 472–479 (2010).
12. Crochet, S. & Petersen, C.C. Correlating whisker behavior with membrane potential in barrel cortex of awake mice. *Nat. Neurosci.* **9**, 608–610 (2006).
13. Poulet, J.F. & Petersen, C.C. Internal brain state regulates membrane potential synchrony in barrel cortex of behaving mice. *Nature* **454**, 881–885 (2008).
14. Goard, M. & Dan, Y. Basal forebrain activation enhances cortical coding of natural scenes. *Nat. Neurosci.* **12**, 1444–1449 (2009).
15. Constantinople, C.M. & Bruno, R.M. Effects and mechanisms of wakefulness on local cortical networks. *Neuron* **69**, 1061–1068 (2011).
16. Gentet, L.J., Avermann, M., Matyas, F., Staiger, J.F. & Petersen, C.C. Membrane potential dynamics of GABAergic neurons in the barrel cortex of behaving mice. *Neuron* **65**, 422–435 (2010).
17. Zagha, E., Casale, A.E., Sachdev, R.N., McGinley, M.J. & McCormick, D.A. Motor cortex feedback influences sensory processing by modulating network state. *Neuron* **79**, 567–578 (2013).
18. Polack, P.O., Friedman, J. & Golshani, P. Cellular mechanisms of brain state–dependent gain modulation in visual cortex. *Nat. Neurosci.* **16**, 1331–1339 (2013).
19. Bennett, C., Arroyo, S. & Hestrin, S. Subthreshold mechanisms underlying state-dependent modulation of visual responses. *Neuron* **80**, 350–357 (2013).
20. Wehr, M. & Zador, A.M. Balanced inhibition underlies tuning and sharpens spike timing in auditory cortex. *Nature* **426**, 442–446 (2003).
21. Zhang, L.I., Tan, A.Y.Y., Schreiner, C.E. & Merzenich, M.M. Topography and synaptic shaping of direction selectivity in primary auditory cortex. *Nature* **424**, 201–205 (2003).
22. Tan, A.Y., Zhang, L.I., Merzenich, M.M. & Schreiner, C.E. Tone-evoked excitatory and inhibitory synaptic conductances of primary auditory cortex neurons. *J. Neurophysiol.* **92**, 630–643 (2004).
23. Wu, G.K., Arbuckle, R., Liu, B.H., Tao, H.W. & Zhang, L.I. Lateral sharpening of cortical frequency tuning by approximately balanced inhibition. *Neuron* **58**, 132–143 (2008).
24. Li, L.Y. *et al.* Differential receptive field properties of parvalbumin and somatostatin inhibitory neurons in mouse auditory cortex. *Cereb. Cortex* published online, doi:10.1093/cercor/bht417(14 January 2014).
25. Sakata, S. & Harris, K.D. Laminar-dependent effects of cortical state on auditory cortical spontaneous activity. *Front. Neural Circuits* **6**, 109 (2012).
26. Zhou, Y. *et al.* Preceding inhibition silences layer 6 neurons in auditory cortex. *Neuron* **65**, 706–717 (2010).
27. Zhou, Y. *et al.* Generation of spike latency tuning by thalamocortical circuits in auditory cortex. *J. Neurosci.* **32**, 9969–9980 (2012).
28. Wu, G.K., Li, P., Tao, H.W. & Zhang, L.I. Nonmonotonic synaptic excitation and imbalanced inhibition underlying cortical intensity tuning. *Neuron* **52**, 705–715 (2006).
29. Sun, Y.J. *et al.* Fine-tuning of pre-balanced excitation and inhibition during auditory cortical development. *Nature* **465**, 927–928 (2010).
30. Dantzker, J.L. & Callaway, E.M. Laminar sources of synaptic input to cortical inhibitory interneurons and pyramidal neurons. *Nat. Neurosci.* **3**, 701–707 (2000).
31. Pfeffer, C.K., Xue, M., He, M., Huang, Z.J. & Scanziani, M. Inhibition of inhibition in visual cortex: the logic of connections between molecularly distinct interneurons. *Nat. Neurosci.* **16**, 1068–1076 (2013).
32. Lima, S.Q., Hromadka, T., Znamenskiy, P. & Zador, A.M. PINP: a new method of tagging neuronal populations for identification during in vivo electrophysiological recording. *PLoS ONE* **4**, e6099 (2009).
33. Ma, W.P. *et al.* Visual representations by cortical somatostatin inhibitory neurons—selective, but with weak and delayed responses. *J. Neurosci.* **30**, 14371–14379 (2010).
34. Jiang, X., Wang, G., Lee, A.J., Stornetta, R.L. & Zhu, J.J. The organization of two new cortical interneuronal circuits. *Nat. Neurosci.* **16**, 210–218 (2013).
35. Winer, J.A. & Larue, D.T. Populations of GABAergic neurons and axons in layer I of rat auditory cortex. *Neuroscience* **33**, 499–515 (1989).
36. Hestrin, S. & Armstrong, W.E. Morphology and physiology of cortical neurons in layer I. *J. Neurosci.* **16**, 5290–5300 (1996).
37. Shlosberg, D., Amitai, Y. & Azouz, R. Time-dependent, layer-specific modulation of sensory responses mediated by neocortical layer 1. *J. Neurophysiol.* **96**, 3170–3182 (2006).
38. Wozny, C. & Williams, S.R. Specificity of synaptic connectivity between layer 1 inhibitory interneurons and layer 2/3 pyramidal neurons in the rat neocortex. *Cereb. Cortex* **21**, 1818–1826 (2011).
39. Glickfeld, L.L., Histed, M.H. & Maunsell, J.H. Mouse primary visual cortex is used to detect both orientation and contrast changes. *J. Neurosci.* **33**, 19416–19422 (2013).
40. Destexhe, A., Rudolph, M. & Pare, D. The high-conductance state of neocortical neurons *in vivo*. *Nat. Rev. Neurosci.* **4**, 739–751 (2003).
41. Haider, B., Hausser, M. & Carandini, M. Inhibition dominates sensory responses in the awake cortex. *Nature* **493**, 97–100 (2013).
42. Liu, B.H. *et al.* Broad inhibition sharpens orientation selectivity by expanding input dynamic range in mouse simple cells. *Neuron* **71**, 542–554 (2011).
43. Xiong, X.R. *et al.* Interaural level difference-dependent gain control and synaptic scaling underlying binaural computation. *Neuron* **79**, 738–753 (2013).
44. Harris, K.D. Top-down control of cortical state. *Neuron* **79**, 408–410 (2013).
45. Poulet, J.F., Fernandez, L.M., Crochet, S. & Petersen, C.C. Thalamic control of cortical states. *Nat. Neurosci.* **15**, 370–372 (2012).
46. Nelson, A. *et al.* A circuit for motor cortical modulation of auditory cortical activity. *J. Neurosci.* **33**, 14342–14353 (2013).
47. Felleman, D.J. & Van Essen, D.C. Distributed hierarchical processing in the primate cerebral cortex. *Cereb. Cortex* **1**, 1–47 (1991).
48. Cauller, L.J., Clancy, B. & Connors, B.W. Backward cortical projections to primary somatosensory cortex in rats extend long horizontal axons in layer I. *J. Comp. Neurol.* **390**, 297–310 (1998).
49. Gonchar, Y. & Burkhalter, A. Distinct GABAergic targets of feedforward and feedback connections between lower and higher areas of rat visual cortex. *J. Neurosci.* **23**, 10904–10912 (2003).
50. Petreanu, L., Mao, T., Sternson, S.M. & Svoboda, K. The subcellular organization of neocortical excitatory connections. *Nature* **457**, 1142–1145 (2009).

ONLINE METHODS

Awake animal preparation. All experimental procedures used in this study were approved by the Animal Care and Use Committee at the University of Southern California. Female C57BL/6J mice aged 5–7 weeks were used in this study. Animals for awake recordings were prepared in a similar way as previously described[43,51]. Mice were housed with 12-h light/dark cycle and with flying saucer pet exercise wheels placed in their home cages. 1 week before the recording, the mouse was anesthetized with isoflurane (1.5%, vol/vol) and a screw for head fixation was mounted on top of the skull with dental cement. An adaptor for connecting to an enclosed sound delivery system was attached to the left ear. Afterward the mouse was injected subcutaneously with 0.1 mg per kg of body weight buprenorphine and returned to its home cage. During the recovery period, the mouse was trained to get accustomed to the head fixation on the recording setup. To fix the head, the screw was tightly fit into a metal post. The animal was allowed to run freely on a flat plate rotating smoothly around its center. On the day of recording, the mouse was anesthetized with isoflurane. Surgery was performed in a sound-attenuation booth (Acoustic Systems). Craniotomy over the A1 region was performed and the dura was removed. The animal was positioned with the left ear connected to a calibrated closed acoustic delivery system using a TDT EC1 speaker. The right ear was plugged. Multiunit recordings were made with a tungsten electrode (2 MΩ, FHC) to identify the A1 based on response properties and the tonotopic gradient, as described in previous studies[52]. The animal head was tilted so that the electrode could penetrate the A1 surface at an angle of 80°. The animal was allowed to recover from isoflurane for at least 1 h. Recording was started after the animal exhibited normal running. The recording session lasted for about 4 h. The animal was given drops of 5% sucrose (wt/vol) through a pipette every hour.

***In vivo* whole-cell and loose-patch recordings in awake animals.** Whole-cell recordings were made with an Axopatch 200B amplifier (Molecular Devices). Patch pipettes (impedance of 4–5 MΩ) contained a cesium-based solution: 125 mM cesium gluconate, 5 mM TEA-Cl, 4 mM MgATP, 0.3 mM GTP, 10 mM phosphocreatine, 10 mM HEPES, 10 mM EGTA, 2 mM CsCl, 1.5 mM QX-314, 1% biocytin (wt/vol) or 0.25 mM fluorescent dextrans, pH 7.3. The patch pipette, controlled by a micromanipulator (Siskiyou), was lowered into the A1 at the same angle as in multiunits recordings. The cortical surface was covered with 3.5% agar prepared in a warm artificial cerebrospinal fluid (ACSF; 124 mM NaCl, 1.2 mM NaH_2PO_4, 2.5 mM KCl, 25 mM $NaHCO_3$, 20 mM glucose, 2 mM $CaCl_2$, 1 mM $MgCl_2$). Whole-cell capacitance was fully compensated and the initial series resistance (R_s, 15–50 MΩ) was compensated for 40–60% to achieve an effective R_s of 10–30 MΩ. For some recordings, we regularly monitored R_s before, during and after epochs of animal movements. The running epochs were relatively evenly spaced during each of recording sessions, which usually last for less than 10 min, enough for us to collect data for different states. There was no substantial change (<10%) of R_s during our effective recording sessions (**Supplementary Figs. 6** and **7**). Signals were low-pass filtered at 2 kHz and sampled at 10 kHz. Only cells with resting membrane potential lower than −50 mV were studied. A −10-mV junction potential was corrected. Excitatory and inhibitory synaptic currents were recorded under the voltage-clamp mode with the cell clamped at −70 mV and 0 mV, respectively. Membrane potentials were recorded under the current-clamp mode with pipettes containing a potassium-based solution: 130 mM potassium gluconate, 4 mM MgATP, 0.3 mM GTP, 8 mM phosphocreatine, 10 mM HEPES, 10 mM EGTA, 5 mM KCl, 1 mM $CaCl_2$, 0.25 mM fluorescein dextran, pH 7.3. Signals were low pass filtered at 5 kHz and sampled at 10 kHz. As demonstrated previously[23,26,53], the blind whole-cell recording method with relatively large pipette openings resulted in almost exclusive sampling from excitatory cortical neurons. Loose-patch recordings were performed as previously described[54], with a pipette filled with ACSF. Signals were recorded in voltage clamp, with a command voltage applied to adjust the baseline current to be zero. Loose-patch recordings from MGBv neurons were made by vertically penetrating the brain (2.8~3.6 mm from Bregma, 1.7~2.2 mm from midline, 2.8~3.2 mm below the pia surface). MGBv was discriminated from other auditory thalamic regions as previously described[54]. LFP recordings were made with the same recording pipette as in loose-patch recordings. During recordings, behaviors of the animal were recorded with a video camera. The rotating speed (without distinguishing the rotation direction) of the plate was detected with an optical sensor and recorded simultaneously. The behavioral and rotating speed recordings were precisely timed with the electrophysiological recording. The behavioral state of the animal was analyzed both online and offline.

On average, one good whole-cell recording (maintained for 20–40 min) or two loose-patch recordings (maintained for more than 1 h) was obtained in each well-trained animal. The recording sites were marked. The laminar locations of the recorded neurons were determined based on the micromanipulator reading, and in some cases confirmed by histology of the track of pipette penetration and/or fluorescence or biocytin labeled cell bodies. We found a relatively good correspondence between the traveling depth of the recording pipette from the pia and the reconstructed laminar location of the recorded neuron (**Supplementary Fig. 2**). The depth range of different layers in mouse A1 was determined based on the results from Nissl staining and fluorescence expression pattern in a L4-specific Cre line (Scnn1a-Tg3-cre; Jackson Laboratory) crossed with the Ai14 reporter mouse (**Supplementary Fig. 2a**). The L2/3 neurons were sampled at a cortical depth of 250–350 μm from the pial surface, L4 neurons at a depth of 375–500 μm[54], and L1 neurons were within 100 μm from the pia.

Optogenetically guided loose-patch recordings from PV neurons. Adult PV-Cre (Jackson Laboratory) female mice were anesthetized with 1.5% isoflurane. A small cut was made on the skin covering the right A1 and the muscles were removed. Two ~0.2-mm craniotomies were made in the A1 region (temporal lobe, 2.7 and 3.2 mm caudal to Bregma). Adeno-associated viruses (AAVs) encoding ChR2 were purchased from the University of Pennsylvania Viral Vector Core: AAV2/9.EF1α.DIO.hChR2(H134R)-EYFP.WPRE.hGH (Addgene 20298). The virus was delivered using a beveled glass micropipette (tip diameter, ~40 μm) attached to a microsyringe pump (World Precision Instruments). Injections were performed at two locations and two depths (300 and 600 μm), at a volume of 100 nl per injection and at a rate of 20 nl min^{-1}. Right after each injection, the pipette was allowed to rest for 4 min before withdrawal. We then sutured the scalp, injected 0.1 mg per kg buprenorphine and returned the mouse to its home cage. Mice were allowed to recover for 3–4 weeks. On the day of recording, loose-patch recordings using pipettes of smaller tip openings (pipette impedance, ~10 MΩ) were performed. An optic fiber connecting to a blue LED source (470 nm, Thorlabs) was positioned close to the cortical surface of the recording site. We actively searched for neurons exhibiting LED evoked spikes, which were identified as PV neurons. After each experiment, that brain was sectioned and imaged to confirm the expression of ChR2-EYFP.

Silencing L1 with TTX. This method was adapted from a previous study[37]. First, we examined the time course of TTX effects in each layer. A glass pipette containing 1 M NaCl was used for recording multiunit spikes. Multiunit recording was made at 70 μm (L1), 250 μm (L2/3) or 425 μm (L4) below the pia surface of the A1. Responses to repetitive 50 dB CF tones (inter-stimulus interval (ISI) = 4 s) were measured before and after TTX application. TTX solution (5 μM) was applied through a glass micropipette (~100-μm opening) attached via polyethylene tubing to a syringe. Each time we loaded ~2 μl TTX in the pipette and applied a very small pressure so that the TTX solution could be gently applied onto the A1 surface. To determine the contribution of L1 activity to gain changes in L2/3, loose-patch recordings were performed in L2/3 or L4 while the behavior and running speed of the animal were simultaneously recorded. Responses to repetitive 50 dB CF tones (ISI = 2 s) were measured before and after TTX application. Spike responses during a ~150-s window after TTX application when L2/3 firing rates became stable were analyzed and compared to responses before TTX application.

Sound stimulation. Software for sound stimulation and data acquisition was custom-developed in LabVIEW (National Instruments). For loose-patch recordings, pure tones (2–32 kHz spaced at 0.1 octave, 50-ms duration, 3-ms ramp) at eight intensities (0–70 dB SPL spaced at 10 dB) were delivered pseudo-randomly. ISI was 0.5 s. Spike TRFs were continuously mapped to obtain TRFs in different states. It took ~2.5 h to map TRFs for more than 50 repetitions, from which we were able to reconstruct TRFs of about ten repetitions for active states. For whole-cell recordings, either best frequency tones at seven sound intensities (10–70 dB SPL spaced at 10 dB) were delivered randomly with ISI = 2 s, or 40-dB tones at 21 frequencies (2–32 kHz, spaced at 0.2 octave) were delivered pseudo-randomly with ISI = 1 s. Thus, data collection was randomized.

Data analysis. We performed data analysis with custom-developed software (MATLAB, MathWorks). Analysis performers were partially blind to the conditions of the experiments, as the data from all the recorded neurons were first pooled together for a randomized batch processing without categorizing the neurons according to their laminar locations.

Behavioral state. The three behavioral states (**Fig. 1b**), quiescence (Q), active without locomotion (A – L) and locomotion (L), were identified based on the body movement and the rotation speed of the plate. In the Q state, there was no obvious body movement and the average rotation speed (in each 1-s epoch) was lower than 0.5 cm s^{-1}. Animal normally stayed in the Q state for more than 70% of the recording time. In the A – L state, the animal showed whisking and/or facial/jaw/paw movements, which caused small back and forth movements of the plate with an average speed below 2 cm s^{-1}. In the L state, the animal ran forward, with the rotating speed consistently above 2 cm s^{-1}. During locomotion, the mouse also whisked. The two active states each took about 10% of the recording time. Well-trained animals spent relatively more time on running. In a typical experiment, quiescence and active states of the animal were intermingled (**Supplementary Fig. 7a**).

Extracellular signals. LFP signals were low-pass filtered at 300 Hz. After fast Fourier transformation of the signal, normalized power spectrum was obtained and power ratio was calculated as the ratio of the area under 1~10-Hz band over that under 20~80-Hz band. Loose-patch recording signals were filtered with a 100–5,000-Hz band-pass filter. Spontaneous firing rates were calculated from spikes within a 200-ms window before tone onsets, or within 6-s segments of records during which only spontaneous spikes were recorded. Spike TRF was determined as the frequency-intensity space where firing rates exceeded the average spontaneous level by 2 s.d. of baseline fluctuations. Evoked firing rates were calculated by subtracting the average spontaneous firing rate. CF was defined as the frequency at which tones evoked a significant spike response with minimum intensity. This minimum intensity was the intensity threshold of TRF. PSTHs were derived from CF tone–evoked responses. Spike response latency was defined as the lag between the stimulus onset and the time point in the PSTH where evoked firing rate exceeded the average spontaneous firing rate by 2 s.d. of baseline activity. SNR was calculated for CF tone–evoked responses as the evoked firing rate within a 50-ms time window following the tone onset divided by the average spontaneous firing rate.

Synaptic responses. Synaptic response traces evoked by the same test stimuli were averaged separately for each behavior state. Synaptic onset latency was determined at the time point where the evoked current exceeded the average baseline by 2 s.d. Peak amplitude was determined by averaging within a 5-ms window centered at the response peak after subtracting baseline current. Charge transfer was calculated by summing up the current values within the evoked response time window after subtracting baseline current. Excitatory and inhibitory synaptic conductances were derived according to $\Delta I = G_e(V - E_e) + G_i(V - E_i)$. ΔI is the amplitude of the synaptic current at any time point after subtracting the average baseline current specific to each behavior state; G_e and G_i are the excitatory and inhibitory synaptic conductance; V is the holding voltage, and E_e (0 mV) and E_i (−70 mV) are the reversal potentials. The clamping voltage V was corrected from the applied holding voltage (V_h): $V = V_h - R_sI$, where R_s is the effective series resistance. By holding the recorded cell at two different voltages (the reversal potentials for excitatory and inhibitory current respectively), G_e and G_i could be resolved from the equation[23,26,29,55,56]. Resting conductance was calculated based on the average baseline currents within a 50-ms window before the onset of evoked currents recorded under two different voltages (−70 mV and 0 mV).

To determine frequency tuning, peak amplitudes of synaptic inputs at different frequencies were fit with an envelope curve using a MATLAB software Envelope 1.1 (developed by L. Wang, MathWorks), as previously described[29]. Total frequency range and BW50% were defined as the bandwidths of the fitted envelope curve at 10% and 50% of maximum level respectively. BF was defined as the frequency corresponding to the maximum of the fitted envelope curve.

Statistics. Shapiro-Wilk test were first applied to exam whether samples had a normal distribution. In the case of a normal distribution, *t* test or ANOVA test was applied. Otherwise, a nonparametric test (Wilcoxon signed-rank test in this study) was applied. Data were presented as mean ± s.d. if not otherwise specified. In this study, all the representative cases are followed by a population summary to demonstrate the repeatability. No statistical test was run to determine sample size a priori. The sample sizes we chose are similar to those used in previous publications. Given that, for many cells, responses of the same recorded neuron in different states were tested for multiple (>10) times, paired *t* test or Wilcoxon signed-rank test was also performed on an individual-cell basis. The results were generally consistent with the group comparison. For the linear regression, both the correlation coefficient (r) and P value were calculated to evaluate the strength and significance of the linear correlation. r values were indicated for individual linear regressions and summarized in **Figures 2g** and **5m**. For all the L2/3 neurons in **Figure 2**, P values for the correlation between responses in two states (similar as in **Fig. 2b**) were all lower than 10^{-9}. P values for the correlation between excitatory and inhibitory responses of the neurons in **Figure 4** (similar as in **Fig. 4g**) were all lower than 10^{-8}. P values for the correlation between synaptic responses in two different states in **Figure 5** were all lower than 10^{-5}.

A **Supplementary Methods Checklist** is available.

51. Olsen, S.R., Bortone, D.S., Adesnik, H. & Scanziani, M. Gain control by layer six in cortical circuits of vision. *Nature* **483**, 47–52 (2012).
52. Guo, W. *et al.* Robustness of cortical topography across fields, laminae, anesthetic states, and neurophysiological signal types. *J. Neurosci.* **32**, 9159–9172 (2012).
53. Li, Y.T., Ibrahim, L.A., Liu, B.H., Zhang, L.I. & Tao, H.W. Linear transformation of thalamocortical input by intracortical excitation. *Nat. Neurosci.* **16**, 1324–1330 (2013).
54. Li, L.Y., Li, Y.T., Zhou, M., Tao, H.W. & Zhang, L.I. Intracortical multiplication of thalamocortical signals in mouse auditory cortex. *Nat. Neurosci.* **16**, 1179–1181 (2013).
55. Borg-Graham, L.J., Monier, C. & Fregnac, Y. Visual input evokes transient and strong shunting inhibition in visual cortical neurons. *Nature* **393**, 369–373 (1998).
56. Anderson, J.S., Carandini, M. & Ferster, D. Orientation tuning of input conductance, excitation, and inhibition in cat primary visual cortex. *J. Neurophysiol.* **84**, 909–926 (2000).

doi:10.1038/nn.3701